scientific reports

Check for updates

OPEN

N-benzyl-N-methyldecane-1-amine derived from garlic ameliorates UVB-induced photoaging in HaCaT cells and SKH-1 hairless mice

Phatcharaporn Budluang[1,6], Ji Eun Kim[2,6], Eun Seo Park[2], Ayun Seol[2], Hee Jeong Jang[1], Moon Sung Kang[1], Yeon Ha Kim[3], Jongdoo Choi[4], Seonghye Kim[4], Suhkmann Kim[4], Minseob Koh[4], Ho Young Kang[3], Bae-Hwan Kim[5], Dong-Wook Han[1], Dae Youn Hwang[2]✉ & Young-Hwa Chung[1]✉

Skin tissue is susceptible to oxidative stress-induced senescence provoked by ultraviolet (UV) exposure in our daily lives, resulting in photoaging. Herein, we explore whether N-benzyl-N-methyldecan-1-amine (BMDA) derived from garlic ameliorates UVB-induced photoaging. To address this issue, HaCaT keratinocytes were exposed to UVB irradiation under BMDA treatment. The presence of BMDA substantially reduced UVB-induced ROS levels in a dose-dependent manner. BMDA administration counteracted UVB-induced senescence in the β-galactosidase assay. Treatment with BMDA also rescued UVB-exposed cells (S phase; from 18.3 to 25.8%) from cell cycle arrest, similar to the level observed in untreated normal cells. These findings might support our observation that elevated levels of γ-H2AX, a DNA damage marker, under UVB exposure were reduced following BMDA administration. Additionally, BMDA treatment indirectly reduced UVB-induced melanin synthesis in melanocytes since BMDA failed to inhibit tyrosinase activity, a crucial enzyme in melanin synthesis. The topical application of BMDA on the skin of SKH-1 hairless mice also diminished wrinkle formation, supported by recovered collagen levels and the thickness of the epidermis and dermis, compared to those of UVB-control mice. Finally, the BMDA treatment diminished the expression of inflammatory cytokine transcripts such as TNF-α, IL-1β, IL-4, and IL-6 in the UVB-exposed skin tissues. This finding is further supported by Immunofluorescence microscopy, which showed a decrease in the expression of TNF-α, and IL-1β during BMDA treatment. Altogether, as BMDA mitigates UVB-induced photoaging by reducing ROS production, protecting against DNA damage, and suppressing inflammatory cytokine production, it has been proposed as an effective anti-photoaging molecule.

Keywords N-benzyl-N-methyldecan-1-amine, UVB, Photoaging, Anti-oxidation, Skin

Abbreviations

BMDA	N-benzyl-N-methyldecan-1-amine
ROS	Reactive oxygen species
UV	Ultraviolet
DCF-DA	Dichlorofluorescein diacetate
PI	Propidium iodide
DNCB	2,4-dinitrochlorobenzene
CPDs	Cyclobutane pyrimidine dimers
8-OHdG	8-hydroxy-2′-deoxyguanine

[1]Department of Cogno-Mechatronics Engineering, Optomechatronics Research Institute, Pusan National University, Busan 46241, Republic of Korea. [2]Department of Biomaterials Science (BK21 FOUR Program), College of Natural Resources and Life Science, Pusan National University, Miryang 50463, Republic of Korea. [3]Department of Microbiology, Pusan National University, Busan 46241, Republic of Korea. [4]Department of Chemistry, Pusan National University, Busan 46241, Republic of Korea. [5]Department of Public Health, Keimyung University, Daegu 42601, Republic of Korea. [6]Phatcharaporn Budluang and Ji Eun Kim contributed equally to this work. ✉email: dyhwang@pusan.ac.kr; younghc@pusan.ac.kr

N-benzyl-N-methyldecan-1-amine (BMDA), derived from garlic, is synthesized through reductive amination and is characterized by a small molecule (261.45 dalton) and a lipophilic compound without a S atom[1]. This is noteworthy, considering that many components of garlic, such as allicin, diallyl sulfide, and ajoene, contain S atoms[1,2]. Our previous study demonstrated that BMDA suppresses cancer-upregulated gene 2 (CUG2)-induced cancer stem cell phenotypes, including rapid cell migration and epithelial–mesenchymal transition. This inhibition is achieved through modulation of TGF-β signaling, particularly at higher concentrations[1]. Furthermore, our recent findings indicate that both BMDA and its derivative exhibit anti-inflammatory activity in models of 2,4-dinitrobenzenesulfonic acid-induced rat colitis and collagen-induced rheumatoid arthritis[2]. This activity is also observed in 2,4-dinitrochlorobenzene (DNCB)-treated atopic dermatitis mice[3].

UV light is categorized into three types based on its wavelength: UVA (320–400 nm), UVB (280–320 nm), and UVC (100–280 nm)[4]. The skin, being the outermost tissue, is readily exposed to UVA and UVB in our daily lives. Among these, UVB is particularly harmful, as it directly affects DNA damage through the formation of cyclobutane pyrimidine dimers (CPDs)[5,6] and indirectly induces the formation of 8-hydroxy-2'-deoxyguanine (8-OHdG), an oxidative DNA damage marker[7]. UV-induced ROS can activate the NLRP3 inflammasome, located in the cytosol and the NF-κB transcription factor, promoting the production of inflammatory cytokines such as TNF-α, IL-1β, and IL-6[8–10]. Ultimately, this inflammation leads to ROS production, creating a vicious cycle.

UV irradiation causes DNA damage in keratinocytes, which in turn induces the secretion of α-melanocyte-stimulating hormone (α-MSH), stimulating neighboring melanocytes more pigment production[11–13]. Melanin formation is a hallmark of UV-induced photoaging, providing protection from further DNA damage. The accumulation of UV-induced DNA damage can lead to cellular senescence and cell cycle arrest, both key features of photoaging, in the skin[14–18]. In addition, photoaging in the skin is characterized by wrinkle formation due to collagen loss and reduced elasticity[19,20].

This study aimed to determine how BMDA derived from garlic could safeguard the skin from UVB-induced photoaging. Our findings revealed that BMDA treatment effectively decreased ROS production and DNA damage induced by UVB irradiation, thereby inhibiting cellular senescence and preventing cell cycle arrest. Furthermore, topical application with BMDA demonstrated protective effects in mice, mitigating photoaging features such as wrinkle formation and thickening of the epidermis and dermis.

Results

BMDA treatment effectively reduces ROS production and DNA damage induced by UVB radiation, leading to the rescue of cells from cellular senescence and cell cycle arrest

Our investigation started to determine whether BMDA possesses anti-oxidative functions during UVB-induced oxidative stress. To achieve this, we initially optimized the concentration of BMDA for HaCaT keratinocytes, ensuring it remained non-toxic to the cells. As depicted in Supplementary Fig. 1A, BMDA treatment exhibited cell viability up to 5 μg/mL, while toxicity became evident at 10 μg/mL for 24 h. However, UVB exposure (48 mJ /cm^2) heightened the cell's sensitivity to BMDA, leading to toxicity at 4 μg/mL (Supplementary Fig. 1B and C). Consequently, we selected 1 and 2 μg/mL concentrations of BMDA for its use under UVB exposure.

We utilized DCF-DA, a probe that responds to ROS by emitting green fluorescence, to assess whether UVB irradiation induces ROS and whether the presence of BMDA diminishes ROS production during UVB exposure. As shown in Fig. 1A, UVB exposure evidently increased ROS production, while administration of BMDA resulted in a dose-dependent reduction in the brightness of green fluorescence. Folic acid was employed as a positive control because it protects cells from DNA damage induced by UV exposure, contributing to anti-photoaging[19,21] Folic acid treatment also decreased UVB-induced ROS production, similar to BMDA administration (Fig. 1A).

Since it is well documented that DNA damage leads to phosphorylation of the histone H2AX, by ATM and ATR, forming γ-H2AX[22,23], we hypothesize whether BMDA administration can alleviate this DNA damage. As shown in Fig. 1B, UVB radiation elevates expression of γ-H2AX protein compared to that of untreated control. However, BMDA treatment effectively decreased the level of γ-H2AX protein expression even during UVB exposure, compared to that of DMSO treatment (Fig. 1B).

Given numerous studies report that UVB irradiation also induces cellular senescence and cell cycle arrest as prominent phenotypes of photoaging[14–18], we are curious whether BMDA could prevent cellular senescence induced by UVB exposure. The β-galactosidase assay has been used to detect cellular senescence[24]. Upon senescence the lysosomal mass is increased, leading to production of a higher level of β-galactosidase[25]. UVB exposure alone enhanced the intensity of the blue color indicating a higher levels of β-galactosidase and an increased number of cells exhibiting blue coloration, suggesting that a greater number of senescent cells (Fig. 2). However, the presence of BMDA diminished the intensity of the blue color and reduced the number of cells (relative percentage of blue color cells 35% and 23% at 1 and 2 μg/ml BMDA, respectively, compared to DMSO treatment under UVB radiation) with a blue color in a dose-dependent manner (Fig. 2). Moreover, these findings led us to investigate whether BMDA possesses the capability to overcome cell cycle arrest caused by UVB exposure. The normal cell population, which was not exposed to UVB, comprised 44.6% at the G0/G1 phase, 24.4% at the S phase, and 30.9% at the G2/M phase. On the other hand, the cell population exposed to UVB showed 43.3% at the G0/G1 phase, 18.3% at the S phase, and 38.4% at the G2/M phase (Fig. 3). In contrast, the cells treated with UVB + BMDA (2 μg/mL) exhibited 43.6% at the G0/G1 phase, 25.8% at the S phase, and 30.3% at the G2/M phase, resembling percentages similar to those of the normal cell population (Fig. 3). This result thus indicates that BMDA could overcome the cell cycle arrest instigated by UVB irradiation.

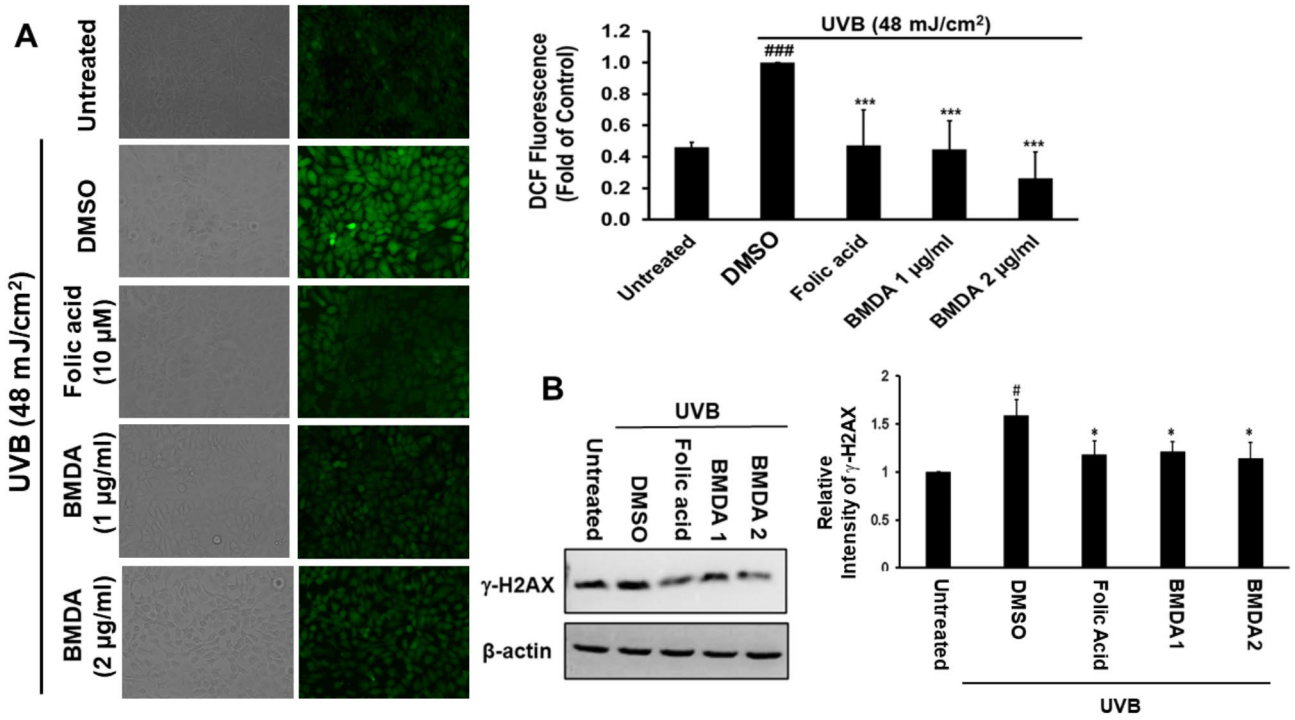

Fig. 1. BMDA treatment diminishes ROS production and DNA damage induced by UVB irradiation. (**A**) HaCaT cells were pre-incubated with folic acid (10 μM) or BMDA addition (1–2 μg/mL) 2 h before UVB radiation. HaCaT cells were exposed to UVB (48 mJ/cm^2) after removing the medium and then cultured for 18 h under folic acid (10 μM) or BMDA addition (1–2 μg/mL). DCF-DA (25 μM) was then added to the medium for 20 min, and the production of ROS was detected under fluorescence microscopy. Three images were captured randomly, and the fluorescence intensity was analyzed using Victor3. ($^{###}p < 0.001$, against "Untreated" group, $^{***}p < 0.001$, against "DMSO" group) (**B**) The cells under the same condition were harvested after UVB exposure for the detection of γ-H2AX using immunoblotting. The cell lysates were separated at 10% SDS-PAGE. γ-H2AX protein was detected with its antibody after transferring the gel to a nitrocellulose membrane. γ-H2AX protein was relatively quantified after scanning of the gel. ($^{#}p < 0.05$, against "Untreated" group, $^{*}p < 0.05$, against "DMSO" group)

The administration of BMDA indirectly suppresses melanin synthesis

We also explored the additional role of BMDA, specifically its potential to inhibit melanin synthesis. This investigation was prompted by the literature that photoaging induced by UVB exposure is characterized by melanin synthesis and accumulation in the skin[2,26,27]. To assess this, we employed B16F1 melanoma cells treated with IBMX, an inhibitor of cAMP/cGMP-dependent phosphodiesterase known to promote melanin synthesis. Initially, we optimized the concentration of BMDA and IBMX to ensure minimal impact on cell toxicity. At both 24 and 48 h post-treatment, IBMX, even at 100 μg/mL, did not significantly affect B16F1 melanoma cell toxicity (Fig. 4A). At 24 h post-treatment, B16F1 cells exhibited nearly 100% viability at up to 4 μg/mL of BMDA and approximately 90% viability at 10 μg/mL (Fig. 4B). Notably, BMDA at concentrations of 2 μg/mL and 4 μg/mL demonstrated approximately 33% and 40% reductions in melanin synthesis, respectively, compared to IBMX treatment alone (Fig. 4C). Furthermore, we sought to determine whether inhibition of melanin synthesis in the presence of BMDA treatment is a result of a direct effect on tyrosinase, a key enzyme in melanin synthesis[28]. To investigate this, we mixed tyrosinase with BMDA at different concentrations (1, 2, and 4 μg/mL) and assessed tyrosinase activity. Remarkably, tyrosinase activity remained unaffected even at the highest concentration of 4 μg/mL (Fig. 4D). These results suggest that BMDA may indirectly impede melanin synthesis rather than directly affect tyrosinase activity.

Topical application of BMDA demonstrates a capacity to mitigate photoaging in hairless mice exposed to UVB light

We extended our investigation to explore whether the anti-oxidation and protection of DNA damage potential observed in vitro for BMDA remains effective in an in vivo setting. SKH-1 hairless mice were used to address this question, and parameters such as wrinkle formation and the thicknesses of the epidermis and dermis were measured. Repeated UVB exposures alone resulted in the deterioration of wrinkle formation compared to the untreated group (Fig. 5A). However, the topical application of BMDA under repetitive UVB irradiation significantly alleviated these phenotypes compared to the Control-UVB or Cream (cream treatment on the skin) groups. Folic acid treatment protected to some extent wrinkle formation (Fig. 5A). Notably, considering that wrinkle formation is often attributed to collagen loss, UVB exposure drastically reduced collagen protein levels

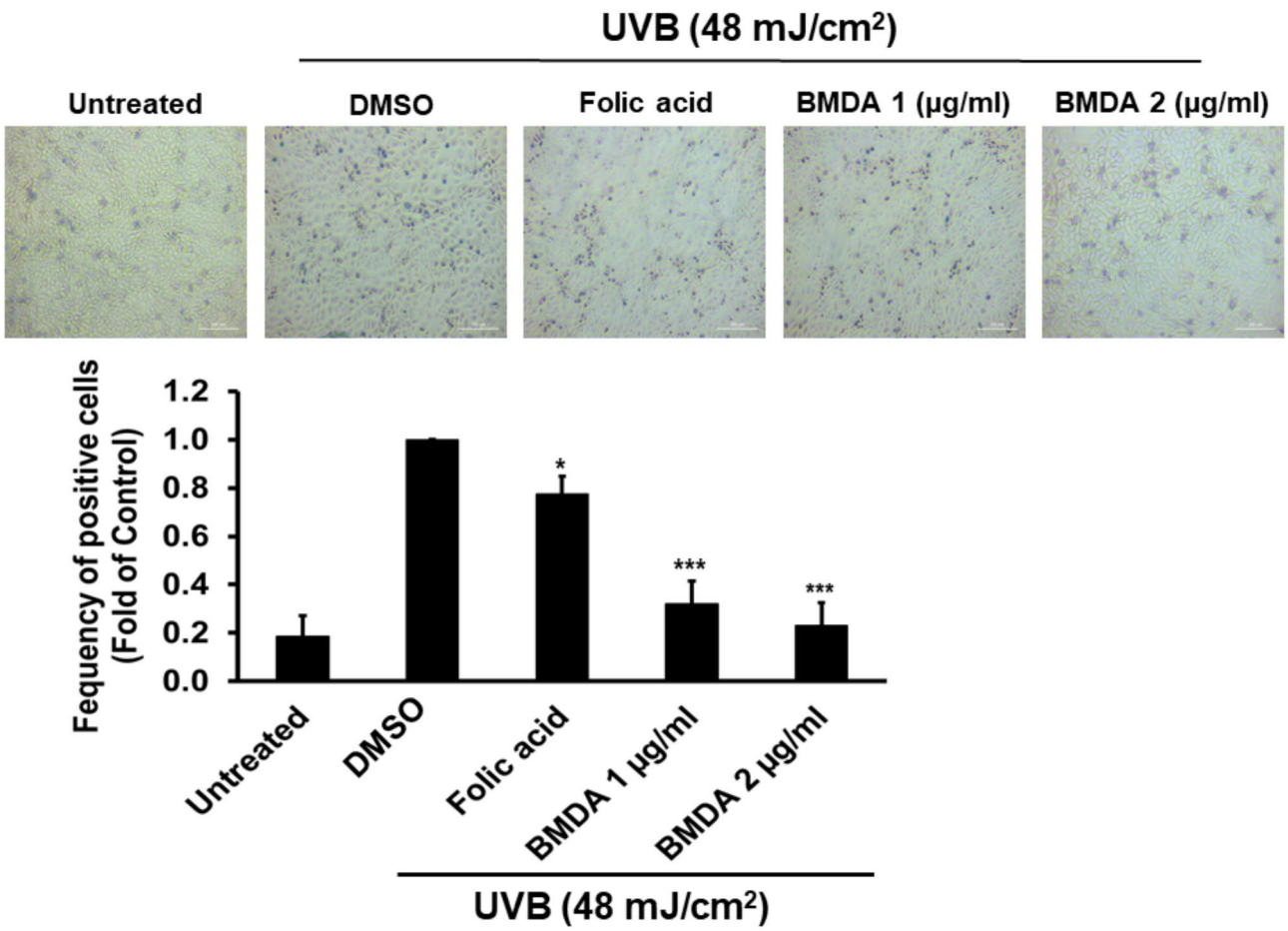

Fig. 2. BMDA application prevents cells from cellular senescence induced by UVB exposure. HaCaT cells were pre-incubated with folic acid (10 μM) or BMDA addition (1–2 μg/mL) 2 h before UVB radiation. HaCaT cells cultured on slide chambers were irradiated with UVB (48 mJ/cm^2) and cultured for 18 h under folic acid (10 μM) or BMDA addition (1–2 μg/mL). According to the manufacturer's protocol, X-gal was added after fixation, and β-galactosidase activity was visualized with a blue color. Three images were captured randomly, and the blue-colored cells were counted. ($^*p < 0.05$, $^{***}p < 0.001$, against "DMSO" group)

and topical application of cream did not prevent degradation of collagen due to UVB radiation (Fig. 5B). However, BMDA treatment inhibited UVB-induced collagen degradation, which demonstrated a restorative effect on the skin even under repeated UVB irradiations (Fig. 5B). Folic acid treatment also showed prevention of collagen degradation induced by UVB rays (Fig. 5B). These results collectively suggest that BMDA possesses a capacity of anti-photoaging including protection of wrinkle formation through resistance to collagen degradation in vivo.

Examining the consequences of BMDA's anti-oxidative effects on the skin of SKH-1 hairless mice, we conducted hematoxylin-eosin staining on the paraffin section and measured skin thickness in animals exposed to UVB light alone and those treated with UVB in conjunction with BMDA. Repeated UVB exposures increased both the epidermis and the dermis thickness, while topical application of BMDA effectively counteracted these effects induced by UVB exposures (Fig. 6A and B). Topical treatment with folic acid could decreased both epidermis and dermis thickness. In addition, we observed that the cream, comprising corn oil and olive wax, slightly impedes the thickening of the dermis induced by repetitive UVB exposure while the cream could not block increase of epidermal thickness due to repeated UVB radiation (Fig. 6A and B).

Topical application of BMDA effectively suppresses the upregulation of inflammatory cytokine transcripts in the skin of hairless mice during UVB-induced oxidative stress

Given the well-documented connection between oxidative stress and inflammation in numerous studies[30–33], we were motivated to investigate whether BMDA treatment could attenuate inflammation in the skin under oxidative stress conditions due to UVB exposure. To answer our question, qRT-PCR was conducted to measure inflammatory cytokine transcripts such as TNF-α, IL-1β, IL-4, and IL-6 in the skin. Following total RNA isolation and cDNA synthesis, PCR was conducted. Repeated UVB exposures elevated the expression of TNF-α, IL-1β, IL-4, and IL-6 transcripts (Fig. 7A and D). However, the BMDA application onto the skin mitigated the expression of these cytokine transcripts under oxidative stress induced by UVB radiation compared to the Control group (Fig. 7A and D). Since cream application also suppressed the expression of the cytokines, the

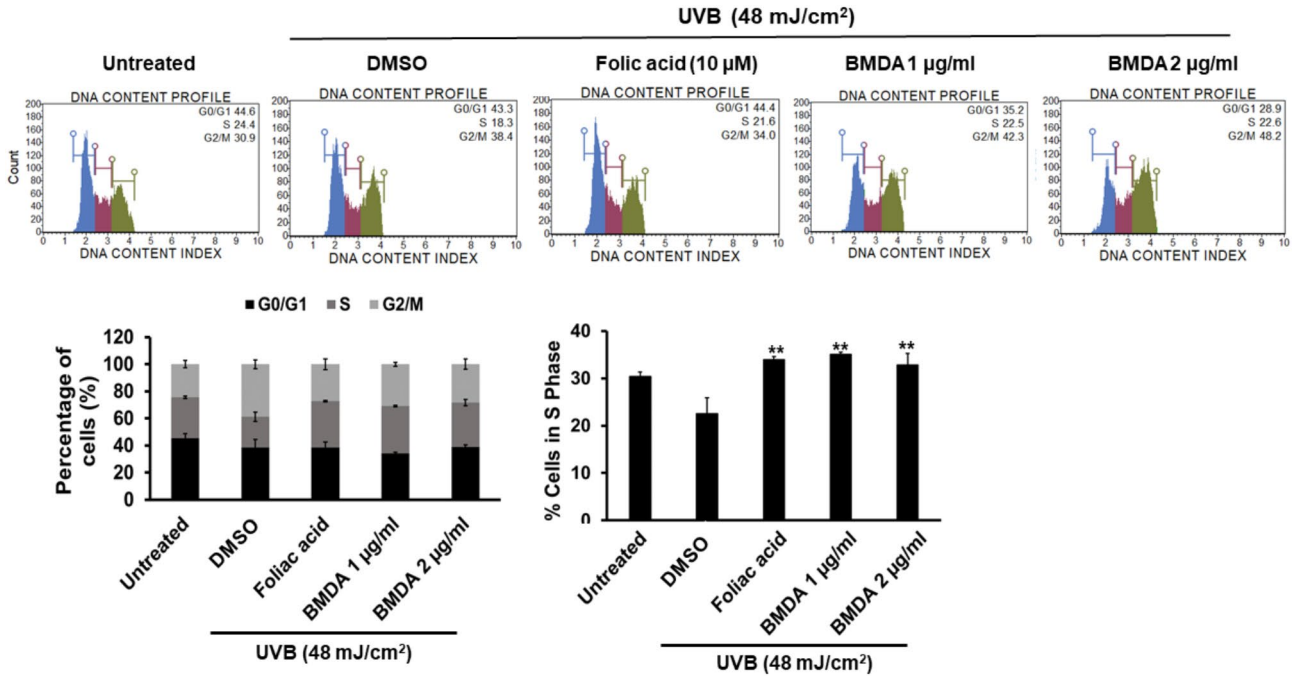

Fig. 3. BMDA treatment relieves UVB-induced cell cycle arrest. HaCaT cells were pre-incubated with folic acid (10 μM) or BMDA addition (1–2 μg/mL) 2 h before UVB radiation. HaCaT cells cultured on slide chambers were irradiated with UVB (48 mJ/cm^2) and cultured for 18 h under folic acid (10 μM) or BMDA addition (1–2 μg/mL). The cells were fixed and permeabilized with 70% cold ethanol for 1 h and resuspended with PI (100 μg/mL). RNase (100 μg/mL) was added for 30 min, and the cell cycles thereafter were analyzed using FAM. Three independent experiments were performed, and the representative FACS data were displayed. (***$p < 0.001$, against "DMSO" group)

cytokine expressions of the BMDA group were compared to those of the Cream group. The IL-1β, IL-6, and IL-4 transcript levels during BMDA treatment under UVB exposures were significantly reduced compared to those in the Cream group, while TNF-α transcript levels were not (Fig. 7A and D). Folic acid application diminished inflammatory cytokine transcripts such as TNF-α, IL-1β, IL-4, and IL-6, compared to those in Control group. When TNF-α, IL-1β and Il-6 transcript levels in Folic acid group were compared with those in Cream group, there were no difference between them except for IL-4 transcript levels. In addition, immunofluorescence microscopy to detect expression of TNF-α and IL-1β protein in the skin tissues exhibited that treatment with BMDA or Folic acid reduces expression of TNF-α and IL-1β in the skin while UVB treatment enhances their expression, which supports qRT-PCR results (Fig. 8). These results underscore the close relationship between UV irradiation and inflammation, consistent with findings from other studies in the literatures[34–36].

Discussion

Our investigation first revealed that BMDA, derived from garlic, exhibits anti-oxidant properties in both HaCaT cells and SKH-1 hairless mice without any structural homology with other garlic components such as allicin[37], diallyl disulfide[38], ajoene[39], and S-allylmercaptocysteine[40], all of which possess anti-oxidative functions. While we demonstrated the anti-oxidative capability of BMDA under oxidative stress induced by UVB exposure, we further explored its potential during TNF-α treatment (Supplementary Fig. 2)[41,42]. Remarkably, BMDA maintained its anti-oxidative function despite the different sources of oxidative stress, highlighting its versatile effectiveness. Subsequently, we will focus on unraveling the molecular mechanism underlying how BMDA can consistently reduce ROS levels across diverse oxidative stress sources. This investigation will be a forthcoming assignment in our research endeavors.

Various natural products have been proposed as anti-oxidants in response to oxidative stress. By carefully examining their chemical structures, they can be categorized as flavonoids, indoles, polyphenols, monoterpenes, and organosulfides[43]. For instance, flavonoids are characterized by two phenyl rings and a heterocyclic ring. This heterocyclic ring contains a carbonyl group (C = O) that can serve as an acceptor for electrons[44]. Indoles, on the other hand, feature a six-membered benzene ring fused to a five-membered pyrrole ring, which carries an alkene (C = C) at positions 2 and 3, imparting electrophilic characteristics[45]. Despite their structural diversity, these natural anti-oxidants share a commonality in having a ketone group or double bond capable of accepting electrons[43]. However, BMDA does not possess these structures because it comprises only a benzene ring and methylamine conjugated with $(CH2)_{10}$. An important question remains: How does BMDA exert an anti-oxidation effect without a carbonyl group or an alkene? Consequently, we assume that BMDA might function indirectly in anti-oxidation systems which will be elucidated by finding a target protein that interacts with BMDA.

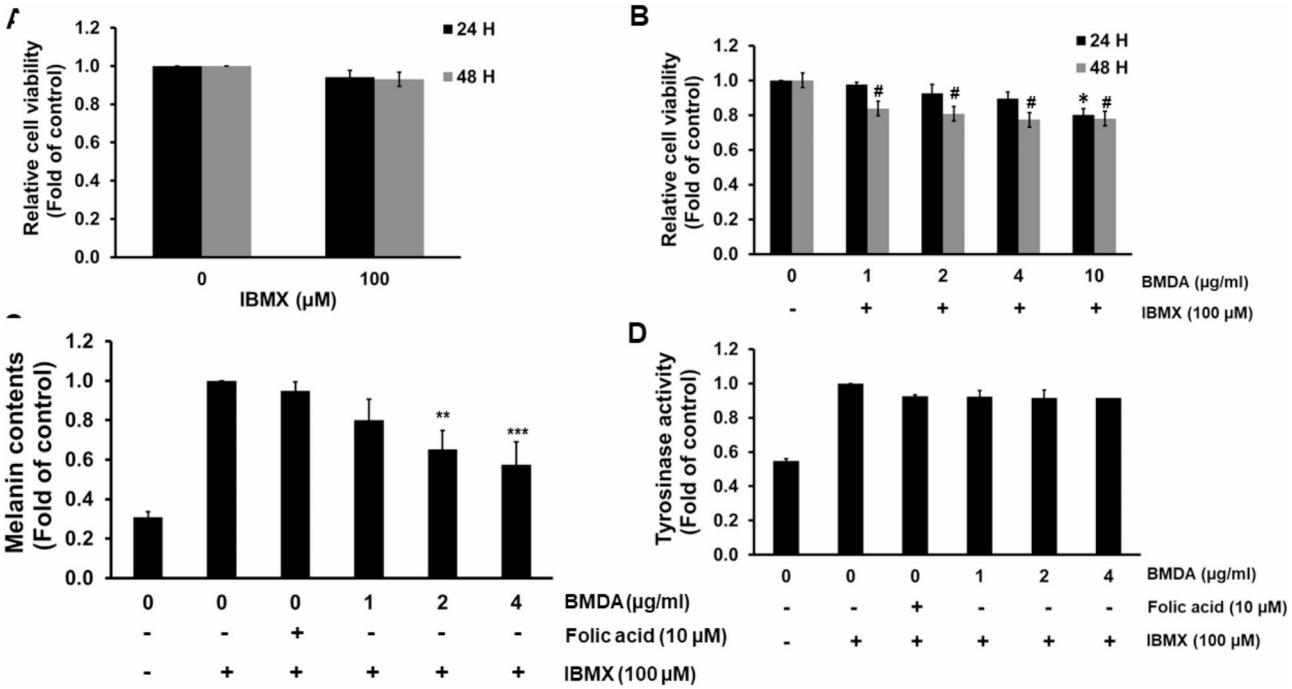

Fig. 4. Treatment with BMDA indirectly decreases melanin synthesis. (**A**) B16 melanoma cells were treated with IBMX at 100 μg/mL for 24–48 h, and the cell viability was measured using an MTT assay. (**B**) The cells were treated with BMDA (1, 2, 4, or 10 μg/mL) in the presence of IBMX (100 μg/mL) for 24–48 h, and the cell viability was examined using an MTT assay. (*$p < 0.05$; against "Untreated" group for 24 h, #$p < 0.05$, against "Untreated" group for 48 h) (**C**) The cells treated with BMDA under IBMX for 24 h were harvested and lysed with 1 N NaOH at 80 °C for 1 h. The melanin contents were measured at 405 nm using a multi-plate reader. (**$p < 0.01$, ***$p < 0.001$, against "Control" group treated with only IBMX) (**D**) The cells treated with BMDA under IBMX for 24 h were harvested and lysed. After centrifugation, the supernatants were incubated with L-DOPA substrate solution (10 mM) at 37 °C for 60 min to calculate tyrosinase activity, and the absorbance was measured at 490 nm.

UV triggers the production of ROS by not only activating NADPH oxidase in the cytoplasm[30,46,47] but also causing respiratory chain reactions in the mitochondria[48–50]. Consequently, these ROS play a pivotal role in promoting inflammation through the activation of NLRP3 inflammasome[8,9] located in the cytosol and NF-κB[30,51–55] for the synthesis of inflammatory cytokines. In addition, UV exposure directly causes formation of CPDs[5,6,56,57] and indirectly 8-OHdG through ROS leading to DNA damage[56,57]. DNA damage further induces to stimulates melanin synthesis from melanocytes through α-melanocyte-stimulating hormone[11–13]. In addition, UVB-induced DNA damage causes cell senescence and cell cycle arrest to fix this danger, which are features of photoaging[14–18]. We therefore propose a diagram to illustrate the mechanism by which BMDA functions in its anti-photoaging against UVB radiation (Fig. 9). However, further investigation is needed to elucidate how BMDA suppresses oxidative stress.

According to a recent study, different outcomes of photoaging has been reported regarding a short-term of UVA or UVB radiation. UVB irradiation induces more severe wrinkle formation compared to UVA exposure[58]. Consistent with this observation, UVB exposure results in a great reduction in collagen levels in the dermis than UVA radiation. Other findings also indicate UVB rays due to higher energy, can cause wrinkle to form earlier and lead to more collagen degradation than UVA[59]. Additionally, UVB exposure causes more severe DNA lesions than UVA radiation while inducing ROS generation to a lesser extent than UVA exposure[59]. Next study will explore how BMDA can delineate its protective effects against UVA and UVB radiation.

Although UVB light primarily affects the epidermis, increases in both epidermal and dermal thickness have been observed in Fig. 6A and B. We speculate that keratinocytes, predominantly located in the epidermis, are influenced by UVB and release inflammatory cytokines in response to UVB-induced ROS, which contribute to the thickening of the epidermis. These inflammatory cytokines also recruit and activate immune cells, resulting in inflammation in the dermis and an increase in its thickness. In our recent study[3], we noted that both epidermal and dermal thickness increased during DNCB treatment. This suggests that DNCB affects both layers almost simultaneously due to a small molecular weight, inducing inflammation at both sites. In contrast, UVB radiation appears to stimulate inflammation sequentially, starting in the epidermis and progressing to the dermis. However, because BMDA has a molecular weight of 261.45 dalton and is an oily molecule, it can easily penetrate both the epidermis and the dermis. This allows it to exert anti-inflammatory effects in the skin comprising the epidermis and dermis from both the DNCB-induced atopic dermatitis model and the UVB-induced photoaging model.

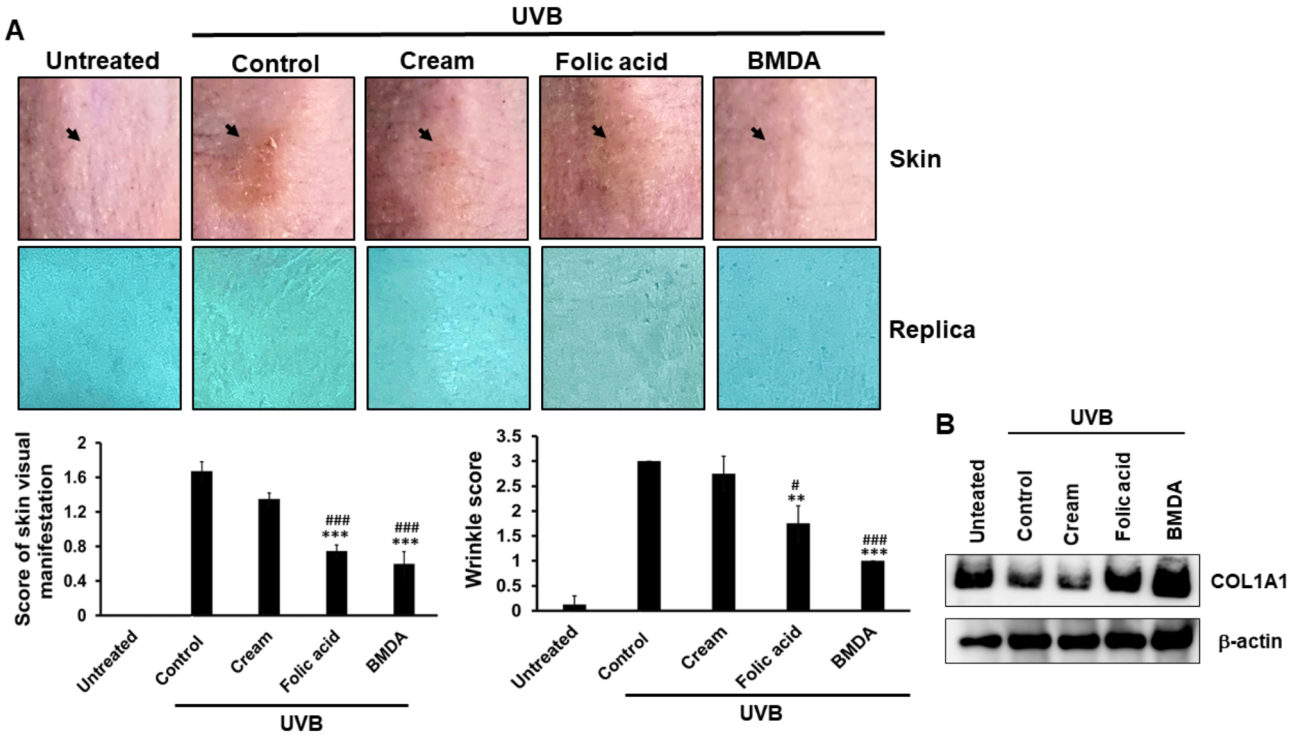

Fig. 5. Topical application of BMDA prevents wrinkle formation on the skin induced by repeated UVB exposure. (**A**) Wrinkle formation on the skin under repetitive UVB irradiation was measured by replica grading after four weeks of BMDA treatment. Wrinkles were evaluated as described previously[29] (grade 0, no wrinkles; grade 1, a few shallow wrinkles; grade 2, some wrinkles; grade 3, several deep wrinkles). (**$p < 0.01$, ***$p < 0.001$, against "Control" group) (#$p < 0.05$, ###$p < 0.001$, against "Cream" group) (**B**) The dorsal skin tissues irradiated by UVB for four weeks were taken and sonicated with RIPA buffer containing 0.1% SDS. After centrifugation, the cell lysates were separated at 6% SDS-PAGE. Collagen I protein was detected with its antibody after transferring the gel to a nitrocellulose membrane.

Materials and methods

Cells and reagents

HaCaT keratinocyte cells and B16 F1 melanoma cells were procured from ATCC (Manassas, VA, USA). The cells were cultured in DMEM medium supplemented with 10% fetal bovine serum, 100 units/mL penicillin, and 100 µg/mL streptomycin at 37 °C in a 5% CO_2 atmosphere.

The antibody against β-actin was obtained from Santa Cruz Biotech (Santa Cruz, CA, USA), while the anti-collagen I antibody was sourced from Cell Signaling Technology (Danvers, MA, USA). IBMX, DCF-DA, and folic acid were acquired from Sigma-Aldrich (St. Louis, MN, USA). BMDA (Molecules & Materials, Daejeon, Korea) was obtained from our previous study[2].

MTT assay

As noted previously[1], HaCaT cells were plated at a density of 5×10^3 cells/200 µl culture medium/well in 96-well microplates. At 24 h of seeding, the cells were subjected to treatments with BMDA, UVB + BMDA, IBMX, or IBMX + BMDA. Subsequently, they were incubated in a medium containing MTT for 4 h and then lysed with DMSO. The quantification of formazan produced from MTT was measured at 570 nm using a microplate reader. Experiments were performed twice and the data shown were the mean values of triplicate wells.

UVB irradiation on the cells

Keratinocyte HaCaT cells were pre-incubated with DMSO as mock, folic acid (10 µM), and BMDA (1–2 µg/mL) for 2 h before UVB irradiation. After the cells were exposed with UVB (48 mJ/cm^2, 306 nm a peak wavelength) using a UV lamp system (UVAB-16, UltraLum, Claremont, CA, USA) containing a UVB lamp (SanKyo-Denki, G6T5E model, Japan), they were further incubated with the medium containing DMSO, folic acid (10 µM), or BMDA (1–2 µg/mL) for 18 h. Thereafter, the cells were analyzed according to their purposes.

Measurement of intracellular ROS

As previously described[60]. HaCaT keratinocytes cells were seeded at 5×10^5 cells/well in 6-well plates and cultured to 70–80% confluency. The cells were pre-incubated with DMSO as mock, folic acid (10 µM), and BMDA (1–2 µg/mL) for 2 h before UVB irradiation. After the cells were treated with UVB + DMSO, UVB + BMDA, or UVB + folic acid for 18 h post-treatment, dichlorofluorescein diacetate (DCF-DA) (Sigma-Aldrich)

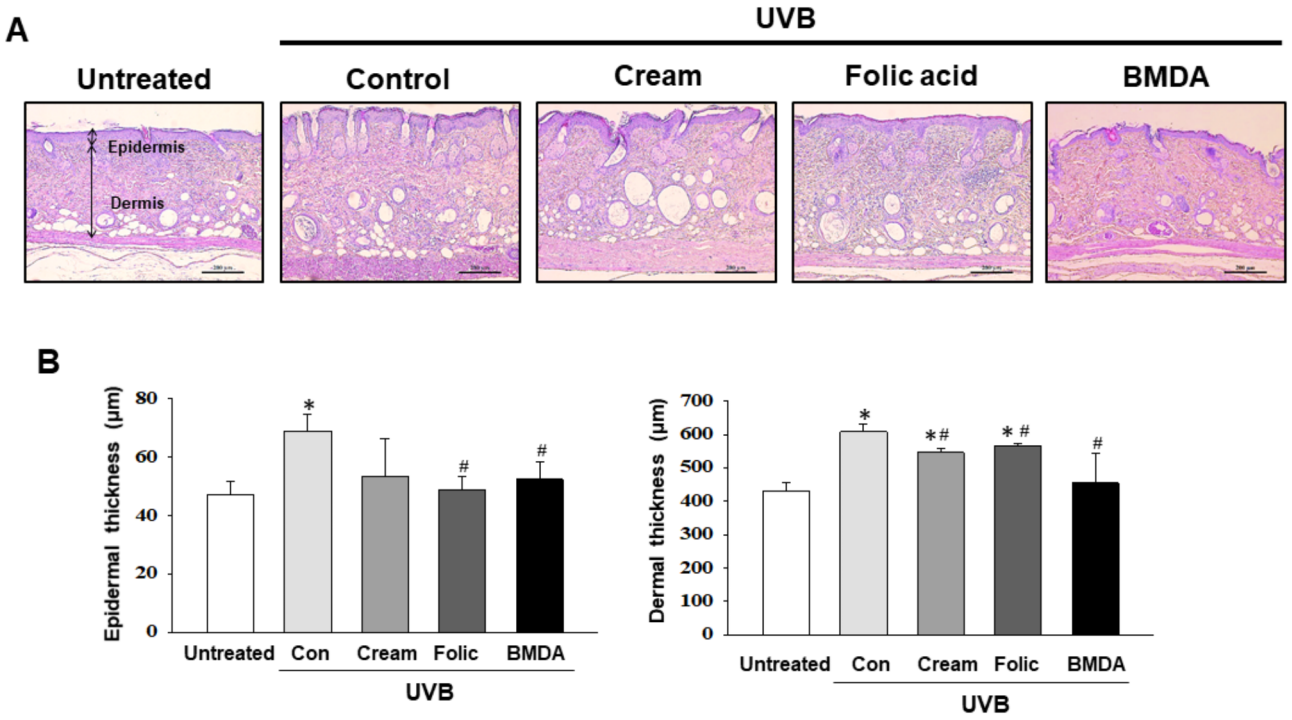

Fig. 6. BMDA treatment interferes with dermis thickening induced by repetitive UVB irradiation. (**A**, **B**) The dorsal skin tissues of the SKH-1 hairless mice irradiated by UVB for four weeks were fixed with 4% paraformaldehyde and stained with hematoxylin and eosin solution after paraffin sectioning. The thicknesses of the epidermis and dermis were measured using the Leica Application Suite (Leica Microsystems). (*$p < 0.05$, against "Untreated" group) (#$p < 0.05$, against "Cream" group).

(25 μM) was added, followed by incubation for 20 min at 37 °C. After washing, the intensity of green fluorescence was observed in DCF-DA-stained cells under a fluorescence microscope (200x Eclipse TX100, Nikon, Tokyo, Japan) and quantitated with Victor3 (PerkinElmer, Waltham, MA, USA). Experiments were performed twice. Data shown are the mean values of triplicate images.

In situ β-galactosidase assay

HaCaT cells were pre-incubated with DMSO as mock, folic acid (10 μM), and BMDA (1–2 μg/mL) for 2 h before UVB irradiation. The cells cultured on a chamber slide (2×10^5 cells/chamber) exposed to UVB + DMSO, UVB + folic acids (10 μM), or UVB + BMDA (1 and 2 μg/mL) were prepared, and the β-galactosidase assay was then performed according to the manufacturer's protocol (Cell Signaling Technology). Cells were washed in PBS (pH 7.4), fixed with 3.7% formaldehyde, and incubated overnight at 37 °C in a freshly prepared staining buffer containing X-gal (1 mg/mL). At the end of the incubation, the cells were washed with H_2O and examined at 200× magnification. Three images were captured randomly, and the blue-colored cells were counted. Experiments were performed twice.

Cell cycle analysis

As depicted previously[60], HaCaT cells were pre-incubated with DMSO as mock, folic acid (10 μM), and BMDA (1–2 μg/mL) for 2 h before UVB irradiation. For cell cycle analysis, the cells (1×10^6 cells) treated with UVB + DMSO, UVB + folic acids (10 μM), or UVB + BMDA (1 and 2 μg/mL) were harvested and fixed with cold 70% ethanol at 4 °C for 1 h. Subsequently, the cells were resuspended with propidium iodide (PI; Sigma-Aldrich, 100 μg/mL) and 100 μg/mL RNase in PBS, followed by incubation at room temperature for 30 min. Flow cytometry was performed, and cell cycle phases were analyzed using FAM (Millipore, Billerica, MA, USA). Data shown are the mean values of three independent experiments.

Measurement of melanin synthesis

As previously described[61], B16F1 melanoma cells (1×10^6 cells) were treated with BMDA (1, 2, and 4 μg/mL) in the presence of IBMX (100 μg/mL) for 24 h. The cells were harvested and lysed with 1 N NaOH at 80 °C for 1 h. Melanin contents from the dissolved solution were measured at 405 nm using a multiple-plate reader (Molecular Device, Sunnyvale, CA, USA). Experiments were conducted twice and the data shown were the mean values of triplicate wells.

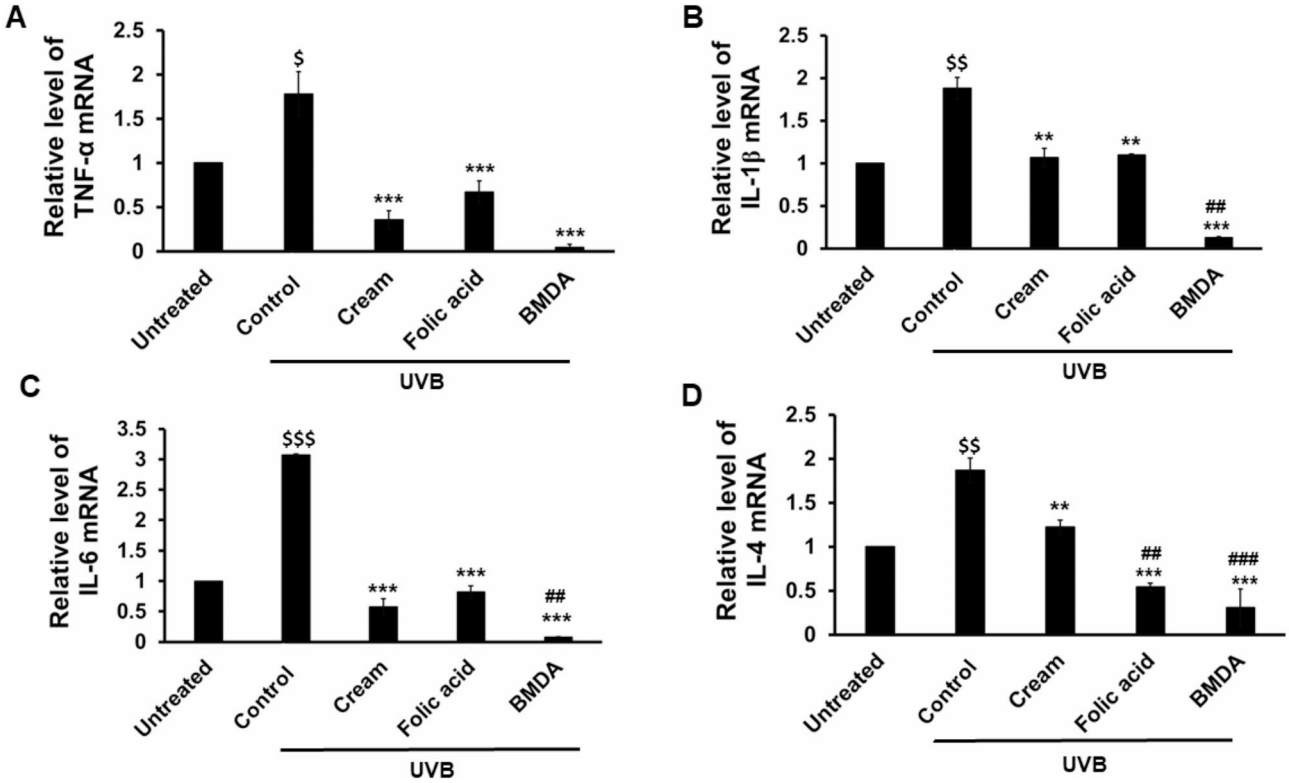

Fig. 7. BMDA treatment diminishes the levels of inflammatory cytokine transcripts during repeated UVB exposures. (**A**–**D**) The total RNAs were isolated from the dorsal skin tissues of the SKH-1 hairless mice under UVB irradiation for four weeks. Quantitative PCR was performed using 2x Power SYBR green and cytokine-specific primers after cDNA synthesis. ($^{\$}p < 0.05$, $^{\$\$}p < 0.01$, $^{\$\$\$}p < 0.001$, against "Untreated" group) ($^{**}p < 0.01$, $^{***}p < 0.001$, against "Control" group) ($\#\#p < 0.01$, $\#\#\#p < 0.001$, against "Cream" group).

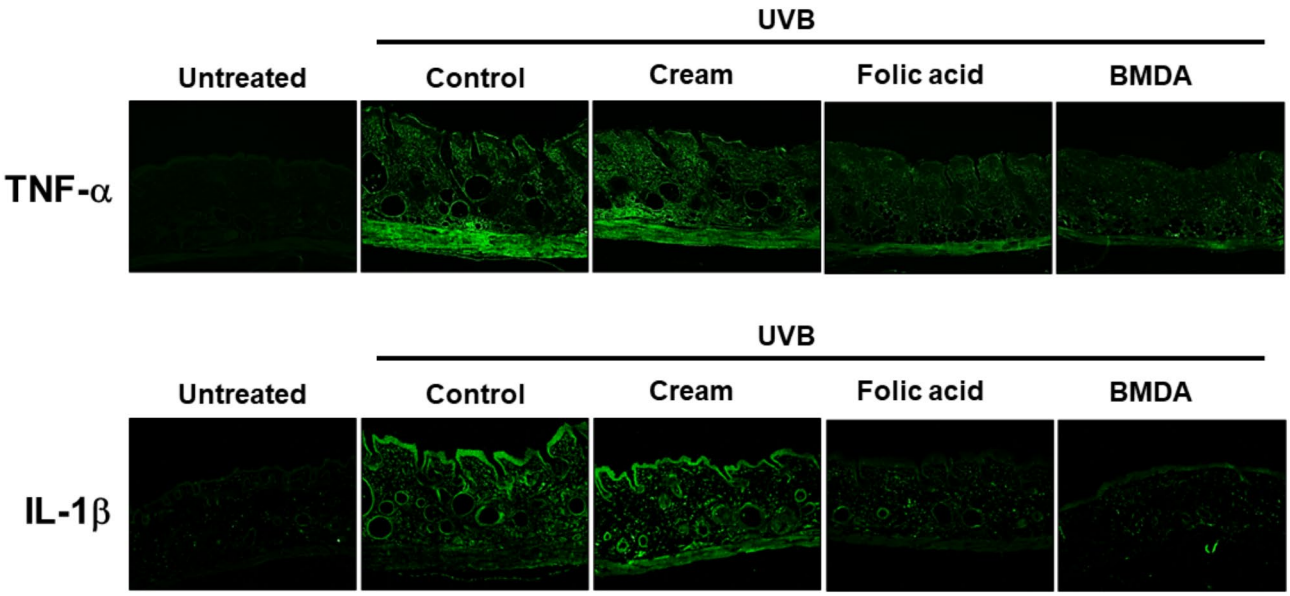

Fig. 8. BMDA treatment reduces protein levels of TNF-α and IL-1β in the skin tissue. Paraffin was removed from paraffin-embedded tissue sections and the tissue was then rehydrated. Tissue antigens were exposed after boiling with unmasking solution and incubated with anti-TNF-α or IL-1β antibody. The fluorescence image was observed under an immunofluorescence microscopy after staining with FITC-conjugated secondary antibodies.

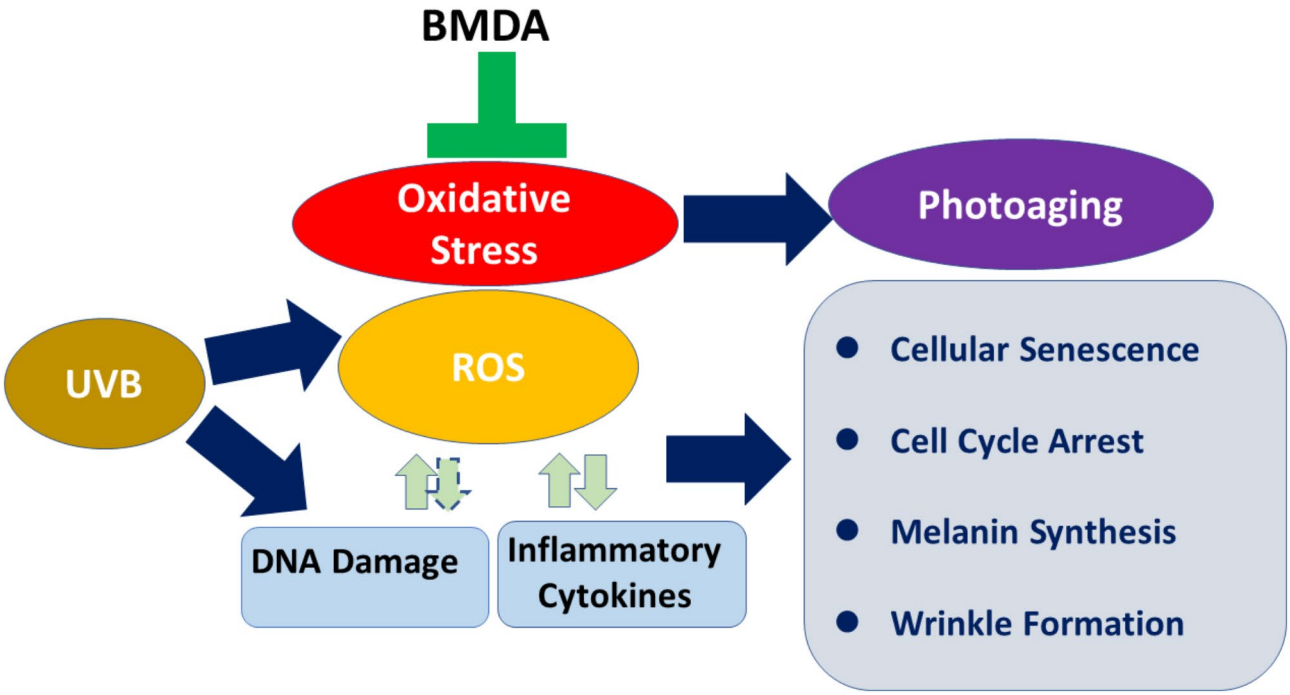

Fig. 9. BMDA exerts its anti-photoaging function under UVB radiation. UVB radiation induces the formation of ROS, leading to DNA damage and the production of inflammatory cytokines that can conversely activate ROS. This oxidative stress contributes to photoaging, manifesting as increased cellular senescence, cell cycle arrest, melanin synthesis, and wrinkle formation. BMDA treatment herein inhibits UVB-induced ROS formation, DNA damage and inflammatory cytokine production, thereby helping to prevent photoaging. (Arrow with solid line: direct effect, Arrow with dotted line: indirect effect)

Measurement of tyrosinase activity

As previously depicted[62], B16F1 melanoma cells (1×10^6 cells) were treated with BMDA (1, 2, and 4 μg/mL) under IBMX (100 μg/mL) addition for 24 h. After the cells were lysed with tritonX-100 (1%) and centrifuged, the supernatants were incubated with L-DOPA (10 mM) as a tyrosinase substrate for 1 h, and the absorbance was measured at 450 nm using a multiple-plate reader (Molecular Device, San Jose, CA, USA). Experiments were performed twice and the data shown were the mean values of triplicate wells.

Western blotting

As previously noted[3], skin tissues or HaCaT cells were sonicated and lysed with lysis buffer containing 0.1% SDS and protease inhibitors (Sigma-Aldrich) for immunoblotting. Proteins from whole cell lysates were resolved by 6–10% SDS-polyacrylamide gel electrophoresis (PAGE) and transferred onto nitrocellulose membranes. Anti-collagen I antibody was used at a 1:1,000 dilution, and anti-rabbit antibodies conjugated with horseradish peroxidase were used at a 1:2,000 dilution in 5% nonfat dry milk. After the final washing, the membranes were evaluated with an enhanced chemiluminescence reagent (Thermo Fisher Scientific, Cambridge, MA, USA) using Image Quant LAS 4000 Mini (GE Healthcare, Piscataway, NJ, USA). Experiments were conducted in triplicate.

Animal care

All animal experiments were conducted following the Laboratory Animal Resources Guide for the Care and Use of Laboratory Animals. Male SKH-1 hairless mice (6 weeks old) were obtained from Central Lab Animal Inc. (Seoul, Korea). They were housed under specific pathogenfree conditions (a 12 h light/12 h dark cycle, at 22 °C and 50–55% humidity) and had free access to both diet and tap water.

Skin photoaging animal model

As previously depicted[63], the dorsal skin of hairless mice was exposed to UVB three times a week using a UV lamp (L20W/12 RS SLV/25, Philips Electronics, Amsterdam, Netherlands), which emits a peak wavelength of 315 nm). The irradiation dose was incremented weekly by MED (1 MED = 130 mJ/cm^2) to 4 MED, and the UVB radiation continued for four weeks. Starting from the initial irradiation, BMDA, folic acid, or vehicle (cream only) was topically administered to the UVB-exposed dorsal skin three times a week for four weeks. Each group consists of 5 animals.

Histopathological analysis

After fixing the dorsal skin of SKH-1 hairless mice in 10% formalin for 48 h, the skin tissues were embedded in paraffin wax as previously described[62]. Subsequently, the paraffin section (4 μm) were sliced onto slide glass,

stained with hematoxylin and eosin (Sigma-Aldrich), and analyzed using light microscopy. The histopathological alterations of the dorsal skin were examined with the Leica Application Suite (Leica Microsystems, Glattbrugg, Switzerland).

Immunofluorescence of paraffin-embedded tissue section

After paraffin was removed using xylene and ethanol, the tissue section was rehydrated with PBS following the previously described protocol[64]. The tissue section was placed in the unmasking solution on a hot plate at 102 °C for 20 min and was cooled down at room temperature. Anti-TNF-α or IL-1β antibody was placed on the tissue section after blocking at 4 °C for overnight and subsequently FITC-conjugated rabbit anti-mouse IgG was incubated at room temperature for 2 h. The image was observed under immunofluorescence microscopy (Axio Observer D1; Zeiss, Oberkochen, Germany).

Wrinkle formation evaluation

As previously depicted[63], each SKH-1 hairless mouse was anesthetized, and the dorsal skin exposed to UVB (wrinkle formation area) was photographed to assess the severity of wrinkling. The severity of wrinkling was measured using Bissett's visual wrinkle scale. Skin impressions (replicas) were created by applying the Repliflo Cartridge Kit (CuDerm Corp., Dallas, TX, USA) to the dorsal skin of each mouse. These replicas were then analyzed using a skin visioline VL650 (CK Electronics GmbH, Cologne, Germany).

Quantitative real-time PCR

As previously noted[3], RT-qPCR was employed to quantify the relative levels of TNF-α, IL-1β, IL-4, and IL-6 mRNAs. After isolation of total RNAs from the skin tissues using RNA Bee solution (Tet-Test Inc., Friendswood, TX, USA), cDNA was synthesized using reverse transcriptase (Superscript II, Thermo Fisher Scientific Inc.). The relative level of the three genes was quantified using 2× Power SYBR Green (Toyobo Co., Osaka, Japan). The primer sequences for the above analyses were as follows: TNF-α, sense 5′-CCT GTA GCC CAC GTC GTA GC-3′ and anti-sense 5′-TTG ACC TCA GCG CTG ACT TG-3′; IL-6, sense 5′-TTG GGA CTG ATG TTG TTG ACA-3′ and anti-sense 5′-TCA TCG CTG TTG ATA CAA TCA GA-3′; IL-1 β, sense 5'-GCA CAT CAA CAA GAG CTT CAG GCA G-3', anti-sense 5'-GCT GCT TGT G AG GTG CTG ATG TAC-3'. IL-4, sense 5′-TAC CAG GAG CCA TAT CCA CGG ATG-3′, anti-sense 5′-TGT GGT GTT CTT CGT TGC TGT GAG-3′. The thermal cycling conditions included a holding stage (1 min at 95 °C), a cycling stage (40 cycles of 15 s at 95 °C, 15 s at 57 °C, and 45 s at 72 °C), and a melt curve stage (15 s at 95 °C and 60 s at 60 °C). Additional analyses such as fluorescence intensity, threshold values, threshold cycle (Ct), and housekeeping genes were conducted, as described in our previous study[23]. Data shown were the mean values of three independent experiments.

Statistical significance

The data were expressed as mean ± standard deviation (SD) and subjected to analysis using one-way ANOVA followed by Tukey's test for comparisons between groups. Error bars on graphs represent SD. A p-value of less than 0.05 was considered statistically significant.

Data availability

Data is provided within the manuscript or supplementary information files. Materials used and /or analyzed during the current study are available from the corresponding author (Y.-H. C.) on reasonable request.

Received: 16 April 2024; Accepted: 29 January 2025
Published online: 26 February 2025

References

1. Kaowinn, S. et al. N-Benzyl-N-methyl-dodecan-1-amine, a novel compound from garlic, exerts anti-cancer effects on human A549 lung cancer cells overexpressing cancer upregulated gene (CUG)2. *Eur. J. Pharmacol.* **841**, 19–27. https://doi.org/10.1016/j.ejphar.2018.09.035 (2018).
2. Kim, J. E. et al. N-benzyl-N-methyldecan-1-amine and its derivative mitigate 2,4- dinitrobenzenesulfonic acid-induced colitis and collagen-induced rheumatoid arthritis. *Front. Pharmacol.* **14**. https://doi.org/10.3389/fphar.2023.1095955 (2023).
3. Kim, J. E. et al. N-benzyl-N-methyldecan-1-amine, derived from garlic, and its derivative alleviate 2,4-dinitrochlorobenzene-induced atopic dermatitis-like skin lesions in mice. *Sci. Rep.* **14**, 6776. https://doi.org/10.1038/s41598-024-56496-2 (2024).
4. Kawashima, S. et al. Protective effect of pre- and post-vitamin C treatments on UVB-irradiation-induced skin damage. *Sci. Rep.* **8**, 16199. https://doi.org/10.1038/s41598-018-34530-4 (2018).
5. Kurz, B., Klein, B., Berneburg, M. & Meller, S. UV-induzierte Pathogenese Des Lupus erythematodes. *Die Dermatol.* **75**, 528–538. https://doi.org/10.1007/s00105-024-05369-w (2024).
6. Garcia-Ruiz, A., Kornacker, K. & Brash, D. E. Cyclobutane pyrimidine dimer hyperhotspots as sensitive indicators of keratinocyte UV exposure. *Photochem. Photobiol.* **98**, 987–997. https://doi.org/10.1111/php.13683 (2022).
7. Lee, J. K., Ko, S. H., Ye, S. K. & Chung, M. H. 8-Oxo-2'-deoxyguanosine ameliorates UVB-induced skin damage in hairless mice by scavenging reactive oxygen species and inhibiting MMP expression. *J. Dermatol. Sci.* **70**, 49–57. https://doi.org/10.1016/j.jdermsci.2013.01.010 (2013).
8. Swanson, K. V., Deng, M. & Ting, J. P. Y. The NLRP3 inflammasome: Molecular activation and regulation to therapeutics. *Nat. Rev. Immunol.* **19**, 477–489. https://doi.org/10.1038/s41577-019-0165-0 (2019).
9. Zhou, R., Yazdi, A. S., Menu, P. & Tschopp, J. A role for mitochondria in NLRP3 inflammasome activation. *Nature* **469**, 221–225. https://doi.org/10.1038/nature09663 (2011).
10. Shen, S., He, F., Cheng, C., Xu, B. & Sheng, J. Uric acid aggravates myocardial ischemia-reperfusion injury via ROS/NLRP3 pyroptosis pathway. *Biomed. Pharmacother.* **133**, 110990. https://doi.org/10.1016/j.biopha.2020.110990 (2021).
11. Nguyen, N. T. & Fisher, D. E. MITF and UV responses in skin: From pigmentation to addiction. *Pigment Cell. Melanoma Res.* **32**, 224–236. https://doi.org/10.1111/pcmr.12726 (2019).

12. Cui, R. et al. Central role of p53 in the suntan response and pathologic hyperpigmentation. *Cell* **128**, 853–864. https://doi.org/10.1016/j.cell.2006.12.045 (2007).
13. D'Orazio, J. A. et al. Topical drug rescue strategy and skin protection based on the role of Mc1r in UV-induced tanning. *Nature* **443**, 340–344. https://doi.org/10.1038/nature05098 (2006).
14. van Oosten, M. et al. Mismatch repair protein Msh2 contributes to UVB-induced cell cycle arrest in epidermal and cultured mouse keratinocytes. *DNA Repair* **4**, 81–89. https://doi.org/10.1016/j.dnarep.2004.08.008 (2005).
15. Tan, C. Y. R. et al. Nicotinamide prevents UVB- and oxidative stress–induced photoaging in human primary keratinocytes. *J. Invest. Dermatol.* **142**, 1670–1681. https://doi.org/10.1016/j.jid.2021.10.021 (2022).
16. Chazal, M. et al. P16(INK4A) is implicated in both the immediate and adaptative response of human keratinocytes to UVB irradiation. *Oncogene* **21**, 2652–2661. https://doi.org/10.1038/sj.onc.1205349 (2002).
17. Feng, J. et al. hnRNP A1 promotes keratinocyte cell survival post UVB radiation through PI3K/Akt/mTOR pathway. *Exp. Cell Res.* **362**, 394–399. https://doi.org/10.1016/j.yexcr.2017.12.002 (2018).
18. Ge, Y. et al. Doxercalciferol alleviates UVB-induced HaCaT cell senescence and skin photoaging. *Int. Immunopharmacol.* **127**, 111357. https://doi.org/10.1016/j.intimp.2023.111357 (2024).
19. Kim, D. J., Iwasaki, A., Chien, A. L. & Kang, S. UVB-mediated DNA damage induces matrix metalloproteinases to promote photoaging in an AhR- and SP1-dependent manner. *JCI Insight* **7**. https://doi.org/10.1172/jci.insight.156344 (2022).
20. Choi, S. I. et al. Eisenia bicyclis extract repairs UVB-Induced skin photoaging in vitro and in vivo: Photoprotective effects. *Mar. Drugs* **19**, 693 (2021).
21. Du, P. et al. Folic acid protects melanocytes from oxidative stress via activation of Nrf2 and inhibition of HMGB1. *Oxid. Med. Cell. Longev.* **2021**, 1608586. https://doi.org/10.1155/2021/1608586 (2021).
22. Burma, S., Chen, B. P., Murphy, M., Kurimasa, A. & Chen, D. J. ATM phosphorylates histone H2AX in response to DNA double-strand breaks. *J. Biol. Chem.* **276**, 42462–42467. https://doi.org/10.1074/jbc.C100466200 (2001).
23. Ward, I. M. & Chen, J. Histone H2AX is phosphorylated in an ATR-dependent manner in response to replicational stress. *J. Biol. Chem.* **276**, 47759–47762. https://doi.org/10.1074/jbc.C100569200 (2001).
24. Dimri, G. P. et al. A biomarker that identifies senescent human cells in culture and in aging skin in vivo. *Proc. Natl. Acad. Sci. U. S. A.* **92**, 9363–9367. https://doi.org/10.1073/pnas.92.20.9363 (1995).
25. Kurz, D. J., Decary, S., Hong, Y. & Erusalimsky, J. D. Senescence-associated (beta)-galactosidase reflects an increase in lysosomal mass during replicative ageing of human endothelial cells. *J. Cell. Sci.* **113**(Pt 20), 3613–3622. https://doi.org/10.1242/jcs.113.20.3613 (2000).
26. Wang, L. et al. Anti-photoaging and anti-melanogenesis effects of fucoidan isolated from *Hizikia fusiforme* and its underlying mechanisms. *Mar. Drugs*. **18**, 427 (2020).
27. Park, Y. J. et al. Senescent melanocytes driven by glycolytic changes are characterized by melanosome transport dysfunction. *Theranostics* **13**, 3914–3924. https://doi.org/10.7150/thno.84912 (2023).
28. Khan, M. T. H. Molecular design of tyrosinase inhibitors: A critical review of promising novel inhibitors from synthetic origins. *Pure Appl. Chem.* **79**, 2277–2295. https://doi.org/10.1351/pac200779122277 (2007).
29. Bissett, D. L., Hannon, D. P. & Orr, T. V. An animal model of solar-aged skin: Histological, physical, and visible changes in UV-irradiated hairless mouse skin. *Photochem. Photobiol* **46**, 367–378. https://doi.org/10.1111/j.1751-1097.1987.tb04783.x (1987).
30. Forrester, S. J., Kikuchi, D. S., Hernandes, M. S., Xu, Q. & Griendling, K. K. Reactive oxygen species in metabolic and inflammatory signaling. *Circ. Res.* **122**, 877–902. https://doi.org/10.1161/circresaha.117.311401 (2018).
31. Dominic, A., Le, N. T. & Takahashi, M. Loop between NLRP3 inflammasome and reactive oxygen species. *Antioxid. Redox Signal.* **36**, 784–796. https://doi.org/10.1089/ars.2020.8257 (2022).
32. El Hadri, K., Smith, R., Duplus, E., El Amri, C. & Inflammation Oxidative stress, senescence in atherosclerosis: Thioredoxine-1 as an emerging therapeutic target. *Int. J. Mol. Sci.* **23**, 77 (2022).
33. Jha, J. C., Ho, F., Dan, C. & Jandeleit-Dahm, K. A causal link between oxidative stress and inflammation in cardiovascular and renal complications of diabetes. *Clin. Sci.* **132**, 1811–1836. https://doi.org/10.1042/cs20171459 (2018).
34. Salminen, A., Kaarniranta, K., Kauppinen, A. & Photoaging UV radiation-induced inflammation and immunosuppression accelerate the aging process in the skin. *Inflamm. Res.* **71**, 817–831. https://doi.org/10.1007/s00011-022-01598-8 (2022).
35. Liu, M. et al. Pyruvate and lactate based hydrogel film inhibits UV radiation-induced skin inflammation and oxidative stress. *Int. J. Pharm.* **634**, 122697. https://doi.org/10.1016/j.ijpharm.2023.122697 (2023).
36. Chhabra, G., Ahmad, N., Trichloroisocyanuric Acid, A Swimming Pool Disinfectant. & New Developments and Role in UV-Induced skin inflammation. *Photochem. Photobiol.* **99**, 869–871. https://doi.org/10.1111/php.13700 (2023).
37. Shan, Y. et al. Allicin ameliorates renal ischemia/reperfusion injury via inhibition of oxidative stress and inflammation in rats. *Biomed. Pharmacother.* **142**, 112077. https://doi.org/10.1016/j.biopha.2021.112077 (2021).
38. Shin, I. S. et al. Diallyl-disulfide, an organosulfur compound of garlic, attenuates airway inflammation via activation of the Nrf-2/HO-1 pathway and NF-kappaB suppression. *Food Chem. Toxicol.* **62**, 506–513. https://doi.org/10.1016/j.fct.2013.09.012 (2013).
39. Kay, H. Y. et al. Ajoene, a stable garlic by-product, has an antioxidant effect through Nrf2-mediated glutamate-cysteine ligase induction in HepG2 cells and primary hepatocytes. *J. Nutr.* **140**, 1211–1219. https://doi.org/10.3945/jn.110.121277 (2010).
40. An, L., Zhao, J., Sun, X., Zhou, Y. & Zhao, Z. S-allylmercaptocysteine inhibits mucin overexpression and inflammation via MAPKs and PI3K-Akt signaling pathways in acute respiratory distress syndrome. *Pharmacol. Res.* **159**, 105032. https://doi.org/10.1016/j.phrs.2020.105032 (2020).
41. Yang, J. H., Hwang, Y. H., Gu, M. J., Cho, W. K. & Ma, J. Y. Ethanol extracts of *Sanguisorba officinalis* L. suppress TNF-α/IFN-γ-induced pro-inflammatory chemokine production in HaCaT cells. *Phytomedicine* **22**, 1262–1268. https://doi.org/10.1016/j.phymed.2015.09.006 (2015).
42. Jayasinghe, A. M. K. et al. 3-Bromo-4,5-dihydroxybenzaldehyde isolated from *Polysiphonia morrowii* suppresses TNF-α/IFN-γ-stimulated inflammation and deterioration of skin barrier in HaCaT keratinocytes. *Mar. Drugs* **20**, 563 (2022).
43. Dunaway, S. et al. Natural antioxidants: Multiple mechanisms to protect skin from Solar Radiation. *Front. Pharmacol.* **9**. https://doi.org/10.3389/fphar.2018.00392 (2018).
44. Heim, K. E., Tagliaferro, A. R. & Bobilya, D. J. Flavonoid antioxidants: Chemistry, metabolism and structure-activity relationships. *J. Nutr. Biochem.* **13**, 572–584. https://doi.org/10.1016/s0955-2863(02)00208-5 (2002).
45. Olyaei, A. & Sadeghpour, M. Chemistry of 3-cyanoacetyl indoles: synthesis, reactions and applications: A recent update. *RSC Adv.* **13**, 21710–21745. https://doi.org/10.1039/D3RA04385A (2023).
46. Bedard, K. & Krause, K. H. The NOX family of ROS-generating NADPH oxidases: Physiology and pathophysiology. *Physiol. Rev.* **87**, 245–313. https://doi.org/10.1152/physrev.00044.2005 (2007).
47. Liu, X. & Song, L. Quercetin protects human liver cells from o,p'-DDT-induced toxicity by suppressing Nrf2 and NADPH oxidase-regulated ROS production. *Food Chem. Toxicol.* **161**, 112849. https://doi.org/10.1016/j.fct.2022.112849 (2022).
48. Gomez, J. et al. Methionine and homocysteine modulate the rate of ROS generation of isolated mitochondria in vitro. *J. Bioenerg. Biomembr.* **43**, 377–386. https://doi.org/10.1007/s10863-011-9368-1 (2011).
49. Sanz, A. et al. Methionine restriction decreases mitochondrial oxygen radical generation and leak as well as oxidative damage to mitochondrial DNA and proteins. *FASEB J.* **20**, 1064–1073. https://doi.org/10.1096/fj.05-5568com (2006).
50. Azzouz, D. & Palaniyar, N. Mitochondrial ROS and base excision repair steps leading to DNA nick formation drive ultraviolet induced-NETosis. *Front. Immunol.* **14**, 1198716. https://doi.org/10.3389/fimmu.2023.1198716 (2023).
51. Lingappan, K. NF-κB in oxidative stress. *Curr. Opin. Toxicol.* **7**, 81–86. https://doi.org/10.1016/j.cotox.2017.11.002 (2018).

52. Kabe, Y., Ando, K., Hirao, S., Yoshida, M. & Handa, H. Redox regulation of NF-kappaB activation: Distinct redox regulation between the cytoplasm and the nucleus. *Antioxid. Redox Signal.* **7**, 395–403. https://doi.org/10.1089/ars.2005.7.395 (2005).
53. Zhao, W., Ma, L., Cai, C. & Gong, X. Caffeine inhibits NLRP3 inflammasome activation by suppressing MAPK/NF-κB and A2aR signaling in LPS-Induced THP-1 macrophages. *Int. J. Biol. Sci.* **15**, 1571–1581. https://doi.org/10.7150/ijbs.34211 (2019).
54. Akhter, N. et al. Endoplasmic reticulum stress promotes the expression of TNF-α in THP-1 cells by mechanisms involving ROS/CHOP/HIF-1α and MAPK/NF-κB pathways. *Int. J. Mol. Sci.* **24**, 15186 (2023).
55. Ouyang, J. et al. PVB exerts anti-inflammatory effects by inhibiting the activation of MAPK and NF-κB signaling pathways and ROS generation in neutrophils. *Int. Immunopharmacol.* **126**, 111271. https://doi.org/10.1016/j.intimp.2023.111271 (2024).
56. Al-Sadek, T. & Yusuf, N. Ultraviolet radiation biological and medical implications. *Curr. Issues Mol. Biol.* **46**, 1924–1942 (2024).
57. Zhang, X., Wu, R. S., Fu, W., Xu, L. & Lam, P. K. Production of reactive oxygen species and 8-hydroxy-2'deoxyguanosine in KB cells co-exposed to benzo[a]pyrene and UV-A radiation. *Chemosphere* **55**, 1303–1308. https://doi.org/10.1016/j.chemosphere.2003.12.004 (2004).
58. Mayangsari, E., Mustika, A., Nurdiana, N. & Samad, N. A. Comparison of UVA vs UVB photoaging rat models in short-term exposure. *Med. Arch.* **78**, 88–91. https://doi.org/10.5455/medarh.2024.78.88-91 (2024).
59. Bahamondes Lorca, V. A. et al. Characterization of UVB and UVA-340 lamps and determination of their effects on ER stress and DNA damage. *Photochem. Photobiol.* **98**, 1140–1148. https://doi.org/10.1111/php.13585 (2022).
60. Kang, E. J. et al. Humulus japonicus extract ameliorates collagen–induced arthritis in mice through regulation of overall articular inflammation. *Int. J. Mol. Med.* **45**, 417–428. https://doi.org/10.3892/ijmm.2019.4417 (2020).
61. Kim, C. S. et al. A potent tyrosinase inhibitor, (E)-3-(2,4-Dihydroxyphenyl)-1-(thiophen-2-yl)prop-2-en-1-one, with anti-melanogenesis properties in α-MSH and IBMX-induced B16F10 melanoma cells. *Molecules* **23**, 2725 (2018).
62. Lee, S. J. et al. Antioxidative role of *Hygrophila erecta* (Brum. F.) Hochr. On UV-Induced photoaging of dermal fibroblasts and melanoma cells. *Antioxidants* **11**, 1317 (2022).
63. Choi, H. J. et al. Therapeutic effects of cold-pressed perilla oil mainly consisting of linolenic acid, oleic acid and linoleic acid on UV-induced photoaging in NHDF cells and SKH-1 hairless mice. *Molecules* **25**, 989 (2020).
64. Zaqout, S., Becker, L. L. & Kaindl, A. M. Immunofluorescence staining of paraffin sections step by step. *Front. Neuroanat.* **14**. https://doi.org/10.3389/fnana.2020.582218 (2020).

Acknowledgements

We would like to thank Editage (www.editage.co.kr) for English language editing.

Author contributions

P.B., H.J.J., M.S.K., Y.H.K., J.C., and S.K. performed in vitro experiments and acquired and analyzed data. J.E.K., E.S.P., A.S., and B.H.K. conducted in vivo experiments, established conditions, and collected data. S.K., M.K., and H.Y.K. oversaw in vitro experiments, interpreted results, and contributed to discussions. D.Y.H. supervised animal experiments, interpreted results, contributed to discussions, and provided study funding. Y.-H.C. organized all experiments, wrote and revised the manuscripts with input from all authors, and provided study funding.

Funding

This study received funding from Hayoung Meditech, Inc. The funder was not involved in the study design, collection, analysis, interpretation of data, the writing of this article or the decision to submit it for publication. All authors declare no other competing interests.

Declarations

Competing interests

The authors declare no competing interests.

Ethical approval

Animal experiments were conducted in compliance with the Laboratory Animal Resources Guide. The protocols for the animal study regarding UV-induced skin aging (PNU-2023-0327) received approval from the Pusan National University Animal Care and Use Committee and adhered to the ARRIVE2.0 guidelines.

Additional information

Supplementary Information The online version contains supplementary material available at https://doi.org/10.1038/s41598-025-88634-9.

Correspondence and requests for materials should be addressed to D.Y.H. or Y.-H.C.